Influence of Solid/Liquid Interfaces on the Microstructure and Stress-Rupture Life of the Single-Crystal Nickel-Base Superalloy NASAIR 100

XIPING GUO, HENGZHI FU, AND JIAHUA SUN

The [001] oriented single crystals of nickel-base superalloy NASAIR 100 with the planar, cellular, coarse-dendritic, and fine-dendritic solid/liquid (S/L) interfaces were prepared, respectively, and their microstructure and stress-rupture behavior at 1050 °C were investigated in both as-cast and solution heat-treated conditions. It was found that in as-cast single crystals of NASAIR 100, microsegregation and γ/γ' eutectic produced in the solidification process increased, γ' size decreased, and γ' shape tended progressively to be cuboidal, with the successive transition of the S/L interface from planar to cellular, then to coarse-dendritic, and finally to fine-dendritic morphology. Furthermore, the solution temperature required to dissolve all as-cast γ' and most of the γ/γ' eutectic increased with the aforementioned successive transition of S/L interfaces. The reprecipitated γ', after solution heat treatment (SHT), was usually fine and cuboidal. However, some W-rich phase was present in the heat-treated dendritic single crystals. Both the planar and the cellular single crystals of NASAIR 100 exhibited no superiority in stress-rupture life, irrespective of the heat-treatment conditions. Instead, the single crystals with dendritic morphology possessed excellent stress-rupture lives, after heat treatment at 1320 °C for 4 hours, followed by air cooling (AC). Perfect γ' rafts with high-average aspect ratios formed during the stress-rupture tests of dendritic single crystals; in contrast, irregularly coarsening structures appeared in both the planar and cellular single crystals. The microstructure and solution behavior were illustrated in detail. Furthermore, the microstructural factors to affect the high-temperature stress-rupture life of the single crystals of NASAIR 100 were also analyzed.

I. INTRODUCTION

ALTHOUGH much work was attracted to develop new single-crystal superalloys in the past two decades,[1–6] the processing techniques of this kind of materials have also been widely investigated to improve creep-rupture properties in the meantime.[7–13] Two examples are that Fritzemeier studied the improvements in microstructure and mechanical properties of the single-crystal superalloy PWA 1480 by high thermal gradient casting and hot isostatic pressing,[7] and Tang *et al.* investigated the influence of withdrawal rates on the high-temperature creep behavior of the single-crystal superalloy DD3.[8] However, most of the previous work[7–10] was performed on single crystals with dendritic solid/liquid (S/L) interfaces during solidification, possibly because of the technical difficulties in preparing single crystals with the planar and cellular S/L interfaces at high thermal gradients. One exception was that Tien and Gamble studied the microstructure and stress-rupture properties of single crystals of Mar-M200 solidified with various S/L interfaces, in 1971.[11] However, little, if any, mechanical benefit was achieved in their single crystals over the columnar-grained structure because of the presence of C, B, Zr, and Hf in this alloy. Khan[10] inferred in 1986 that planar single crystals should have superior stress-rupture properties, because of the very low microsegregation in the samples. In China, some research work is consistent with this inference of Khan's, but no detailed experiment has been conducted to verify it so far.[13] The purpose of the present work was to prepare the [001] oriented single crystals of NASAIR 100, respectively, with the planar, cellular, coarse-dendritic, and fine-dendritic S/L interfaces, and furthermore, to examine their microstructure and stress-rupture behavior at 1050 °C.

II. EXPERIMENTAL PROCEDURES

The master alloy NASAIR 100 was melted in a vacuum induction furnace. The chemical analysis of the material used is presented in Table I.

Figure 1 exhibits the schematic drawing of the liquid-metal cooling (LMC) directional solidification system, which can produce high thermal gradients. The chamber pressure and temperature were 0.133 Pa and 1590 °C, respectively. The thermal gradient in the liquid just ahead of the S/L interface, G_L, was 250 ± 5 °C/cm. The withdrawal rate was controlled by a minicomputer. The Al_2O_3 crucibles with a 7.8-mm diameter and a 90-mm length were mounted and sealed on the withdrawal bar with refractory materials. The single crystals with various S/L interfaces were produced using a ''seed'' technique, and the seed orientation was [001]. The S/L interfaces during directional solidification were fixed by quenching several samples into the liquid Ga-In-Sn pool. All specimens for microstructural examination and mechanical tests were prepared from the middle parts of single-crystal bars. Some specimens were

XIPING GUO, Associate Professor of Metallurgy and Materials Science, and HENGZHI FU, Professor and Academician of China Academy of Engineering, are with the State Key Laboratory of Solidification Processing, Northwestern Polytechnical University, Xi'an 710072, People's Republic of China. JIAHUA SUN, Senior Engineer and Professor, is with the Department of Superalloys, Central Iron and Steel Research Institute, Beijing 100081, People's Republic of China.

Manuscript submitted December 7, 1995.

Table I. Chemical Analysis of NASAIR 100 (Weight Percent)

Elements	Contents
Al	5.78
Ti	1.22
W	10.14
Mo	1.09
Cr	8.50
Ta	3.30
Ni	bal

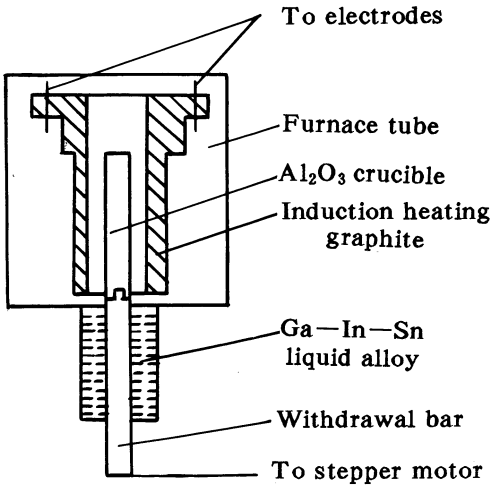

Fig. 1—Schematic drawing of the LMC directional solidification system.

given one of the three heat treatments (1280 °C, 1300 °C, or 1320 °C for 4 hours, followed by air cooling (AC)) before machine work.

Stress-rupture tests were conducted at 1050 °C, and an engineering stress of 160 MPa was employed on specimens with a 6-mm diameter and a 40-mm gauge length, in accordance with ASTM Specification E-8. Two or three specimens were tested for each material condition. The etchant for metallographic examination was a solution of 1.5 g $CuSO_4$ in 40 mL HCl and 20 mL C_2H_5OH. The microstructure was examined in an optical microscope and in a scanning electron microscope (SEM) with energy-dispersive spectroscopy (EDS) detectors. The amount (in area percent) of γ/γ' eutectic, the amount of W-rich phase, and the average edge length of γ' precipitates were determined from quantitative metallography measurements on polished and etched specimens.

III. RESULTS AND DISCUSSION

A. *Solid/Liquid Interfaces and Their Characteristics*

The S/L interface during unidirectional solidification can be controlled by the G_L/R ratio, where G_L is the thermal gradient in the liquid ahead of S/L interfaces, and R is the solidification rate. When G_L was 250 ± 5 °C/cm, the single crystals of NASAIR 100 with the planar, cellular, coarse-dendritic, and fine-dendritic S/L interfaces were produced, respectively, by gradually increasing R. Figure 2 shows the various quenched S/L interfaces. The determination of cell or primary dendrite arm spacing (DAS), λ_1, and secondary DAS, λ_2, is presented in Table II and shown in Figure 3 plotted against the solidification cooling rate, $G_L \cdot R$. The λ_1 and λ_2 of dendrites decreased linearly with increasing $G_L \cdot R$ in the double logarithmic plots. Two linear regressions were conducted on the data of dendrites in Table II, and results were obtained when $G_L \cdot R$ was larger than 3.88×10^{-1} °C/s, as follows:

$$\lambda_1 = 137.4\ (G_L \cdot R)^{-0.285} \quad [1]$$

and

$$\lambda_2 = 31.9\ (G_L \cdot R)^{-0.314} \quad [2]$$

Both confidence levels for Eqs. [1] and [2] were in excess of 95 pct. Figure 3 also exhibits that the cell arm spacing was obviously smaller than the λ_1 of the coarse dendrite. This indicates that a maximum of λ_1 may occur near the transition of the S/L interface from the cellular to the dendritic structure.

B. *As-Cast Microstructure*

Figure 4 illustrates the influence of the solidification cooling rate, $G_L \cdot R$, on Al, Ti, and W segregation ratios, and on the amount of γ/γ' eutectic in the as-cast microstructure, where the segregation ratio of one element was determined as the extreme concentration in interval areas over that in crystallizing cores of this element. With increasing $G_L \cdot R$, the segregation ratios of positive segregation elements Al and Ti increased, while the segregation ratio decreased for W, a negative segregation element. This indicated that microsegregation became serious as the S/L interfaces turned from the planar to the cellular, coarse-dendritic, and finally to the fine-dendritic morphology, successively. Additionally, the amount of γ/γ' eutectic also increased with increasing $G_L \cdot R$, in good correspondence with microsegregation. No γ/γ' eutectic was observed in the planar single crystals of NASAIR 100.

The relationships between the sizes and morphologies of γ' in the as-cast single crystals of NASAIR 100 and $G_L \cdot R$ are shown in Figure 5 and presented in Table III, together with the amount of γ/γ' eutectic. The γ' precipitates were very large and irregularly shaped, in both the planar and cellular single crystals. However, the particles were much smaller and were close to cubic shape in the coarse-dendritic single crystals. The cuboidal and finest γ' precipitates were present in the fine-dendritic single crystals. The γ' precipitates were obviously smaller and more regularly shaped in crystallizing (cellular or dendritic) cores than in interval areas.

C. *Heat-Treated Microstructure*

In the planar single crystals of NASAIR 100, all as-cast γ' precipitates were taken into solution by the 4-hour heat treatment at 1280 °C, and then dispersed cuboidal γ' with an average edge length of about 0.33 μm reprecipitated upon AC (Figure 6(a)). After heat treatment at 1300 °C for 4 hours, and AC, the average edge length of cuboidal γ' was about 0.36 μm. However, at 1320 °C for 4 hours, AC treatment produced a lot of irregular blocks with an average size of about 1.7 μm, besides the cuboidal γ' precipitates with an average edge length of about 0.42 μm, as shown by the arrows in Figure 6(b). Energy-dispersive spectros-

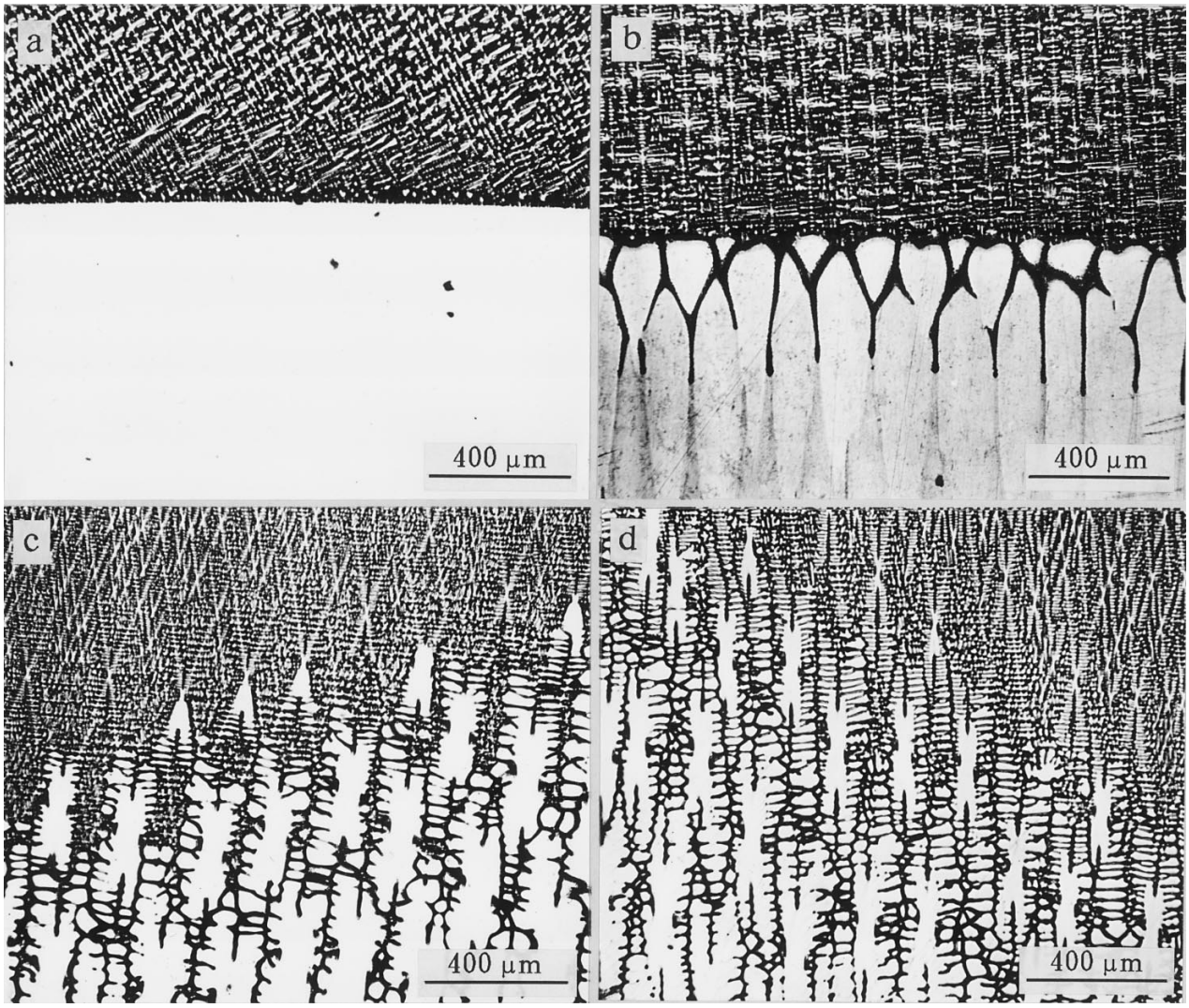

Fig. 2—Optical micrographs showing various quenched S/L interface morphologies, G_L = 250 °C/cm. (*a*) Planar, R = 1.5 μm/s; (*b*) cellular, R = 2.9 μm/s; (*c*) coarse-dendritic, R = 15.5 μm/s; and (*d*) fine-dendritic, R = 87 μm/s.

copy analysis in a SEM revealed that the composition of these observed blocks was 5.6Al, 9.3W, 0.2Mo, 1.2Ti, 5.8Cr, 5.5Ta, and 72.4Ni (in wt pct). Therefore, the large and irregular blocks were still γ' precipitates.

In the cellular single crystals of NASAIR 100, the amount of γ/γ' eutectic reduced to about 0.5 pct after heat treatment at 1280 °C for 4 hours, and AC. The coarse as-cast γ' precipitates in cellular cores had been completely dissolved at 1280 °C, and then cuboidal γ' with an average edge length of about 0.33 μm reprecipitated upon AC (Figure 7(a)); however, the larger as-cast γ' precipitates in cellular intervals had only been partially dissolved at 1280 °C for 4 hours, and the average size of the undissolved γ' precipitates was still about 4.2 μm, as in the as-cast microstructure. However, the reprecipitated γ' in cellular intervals after this heat treatment was cuboidal and very small, with an average edge length of about 0.17 μm (Figure 7(b)). After heat treatment at 1300 °C for 4 hours, and AC, all as-cast γ/γ' eutectic and γ' precipitates had been thoroughly dissolved, then γ' cubes with nearly uniform edge length of about 0.33 μm were reprecipitated in both cellular cores and intervals. The average edge length of reprecipitated γ' cubes was increased to about 0.53 μm by heat treatment at 1320 °C for 4 hours, and AC (Figure 7(c)).

In the coarse-dendritic single crystals of NASAIR 100, about 0.8 pct γ/γ' eutectic remained, and the dendritic patterns that indicated microsegregation were still clear after heat treatment at 1280 °C for 4 hours, and AC (Figure 8(a)). Moreover, the as-cast γ' precipitates in interdendritic areas were only partially dissolved during the 4-hour holding at 1280 °C. After heat treatment at 1300 °C for 4 hours, and AC, the amount of γ/γ' eutectic reduced to about 0.3 pct, all as-cast γ' precipitates had been dissolved, and the edge length of reprecipitated γ' cubes in interdendritic areas was almost the same as that in dendrite cores, with a statistical value of about 0.38 μm (Figure 8(b)). After heat treatment at 1320 °C for 4 hours, and AC, the amount of retained γ/γ' eutectic was about 0.1 pct, and the average edge length of reprecipitated γ' was 0.57 μm (Figure 8(c)). Moreover, the samples after this heat treatment were almost segregation free, because no clear dendritic patterns were revealed by etching (Figure 8(d)).

In the fine-dendritic single crystals of NASAIR 100, the amount of γ/γ' eutectic reduced slightly, and was about 6.3

Table II. Cell and Dendrite Arm Spacings of NASAIR 100

Cooling Rate $G_L \cdot R$ (°C/s)	S/L Interface	λ_1 (μm)	λ_2 (μm)
3.75×10^{-2}	planar*	—	—
7.25×10^{-2}	cellular*	145.4	—
		146.7	—
		146.6	—
3.88×10^{-1}	coarse-dendritic*	175.8	41.8
		180.4	43.3
		183.3	43.4
1.05	intermediate-dendritic	130.5	30.1
		135.7	32.4
		141.0	33.0
2.18	fine-dendritic*	107.1	24.2
		110.5	24.8
		112.4	25.6

*Four S/L interfaces were used to examine the structure and stress-rupture properties.

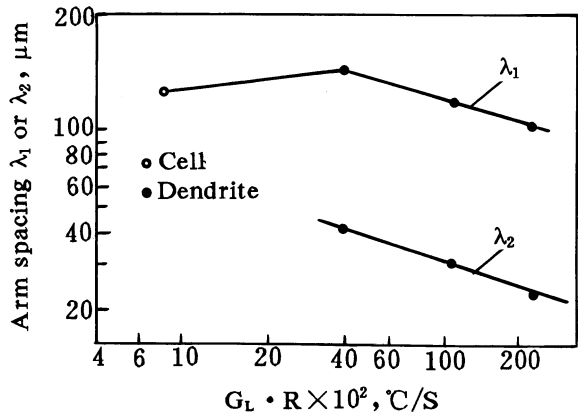

Fig. 3—Relationships of λ_1 and λ_2 to the solidification cooling rate, $G_L \cdot R$.

pct, the as-cast γ' precipitates in dendrite cores had been completely dissolved, and the average edge length of reprecipitated γ' cubes was about 0.30 μm after heat treatment at 1280 °C for 4 hours, and AC. But only a little as-cast γ' was dissolved in interdendritic areas after this treatment (Figure 9(a)). After heat treatment at 1300 °C for 4 hours, and AC, the amount of γ/γ' eutectic decreased about one absolute percent to 5.7 pct; however, the dendritic microsegregation was still serious, as indicated by the dendrite morphology in Figure 9(b). The uniform cuboidal γ' with an edge length of 0.35 μm was reprecipitated in dendrite cores upon AC of this solution treatment. However, the as-cast γ' precipitates in interdendritic areas had still been partially dissolved by the 4-hour heat treatment at 1300 °C, and so the average edge length of undissolved γ' was still 0.45 μm. After heat treatment at 1320 °C for 4 hours, and AC, about 2.2 pct γ/γ' eutectic was retained, and its size was also decreased significantly. However, some residual segregation still remained, because the dendritic patterns were also revealed by etching (Figure 9(c)). All as-cast γ' had been completely taken into solution during the 4-hour holding at 1320 °C. The edge length of reprecipitated γ' in interdendritic areas was almost the same as that in dendrite cores, and the average value was about 0.56 μm (Figure 9(d)).

Another microstructural change due to solution heat treatment (SHT) was the presence of the third phase in dendritic single crystals. Figure 10 illustrates that a relatively large platelike phase with sharp edges was initiated in both the γ/γ' eutectic and the dendrite core areas near the γ/γ' eutectic after SHT. Energy-dispersive spectroscopy analysis in a SEM revealed that the tungsten content in this phase was extremely high, with an overall composition of 2.5Al, 0.2Ti, 3.2Mo, 1.5Cr, 10.2Ni, and 82.4W (in wt pct). No third phase, such as the W-rich phase, was observed in the planar and cellular single crystals of NASAIR 100 (Figures 6 and 7).

The amount of W-rich phase formed during SHT increased with increasing microsegregation produced in the directional solidification processes and with decreasing solution temperatures. The heat treatment at 1280 °C for 4 hours, and AC for the fine-dendritic single crystals produced the most W-rich phase, about 5.0 pct (Figure 10(b)). In addition, about 3.5 pct of the W-rich phase was produced after heat treatment at 1300 °C for 4 hours, and AC, and about 0.3 pct of the W-rich phase was produced after heat treatment at 1320 °C for 4 hours, and AC, in the fine-dendritic single crystals. In the coarse-dendritic single crystals, the amount of W-rich phase produced was about 2.4 pct after heat treatment at 1280 °C for 4 hours, and AC, about 0.7 pct after heat treatment at 1300 °C for 4 hours, and AC, and about 0.1 pct after heat treatment at 1320 °C for 4 hours, and AC (Figure 10(c)).

From the aforementioned experimental results, it can be concluded that the $G_L \cdot R$ value during directional solidification exerted a significant influence on the solution behavior and heat-treated microstructure of the single crystals of NASAIR 100. One important phenomenon was that the solution temperature required to dissolve all as-cast γ' precipitates and most γ/γ' eutectic, and to homogenize compositional microsegregation, increased with the successive transition of S/L interfaces from the planar to the cellular, coarse-dendritic, and finally to the fine-dendritic morphology, when holding time at each temperature was constantly 4 hours (Figure 11).

D. *High-Temperature Stress-Rupture Life*

The stress-rupture lives at 1050 °C and 160 MPa of the single crystals of NASAIR 100, some of which were solution heat treated, are presented in Figure 12, plotted against the S/L interfaces during the unidirectional solidification process. The data are also tabulated in Table IV, together with the corresponding initial microstructure in order to more easily grasp their relationships. The average stress-rupture life of two or three specimens with the same material conditions was used for both accuracy and convenient comparison. In the as-cast condition, the fine-dendritic single crystals exhibited the longest average stress-rupture life (146 hours); however, the average was the shortest, and was 37 hours for the cellular single crystals. Only suitable SHT can improve the stress-rupture life. For example, the heat treatment at 1300 °C for 4 hours, and AC, significantly improved all average stress-rupture lives of the planar, cellular, and coarse-dendritic single crystals, but lowered that of the fine-dendritic single crystals. After

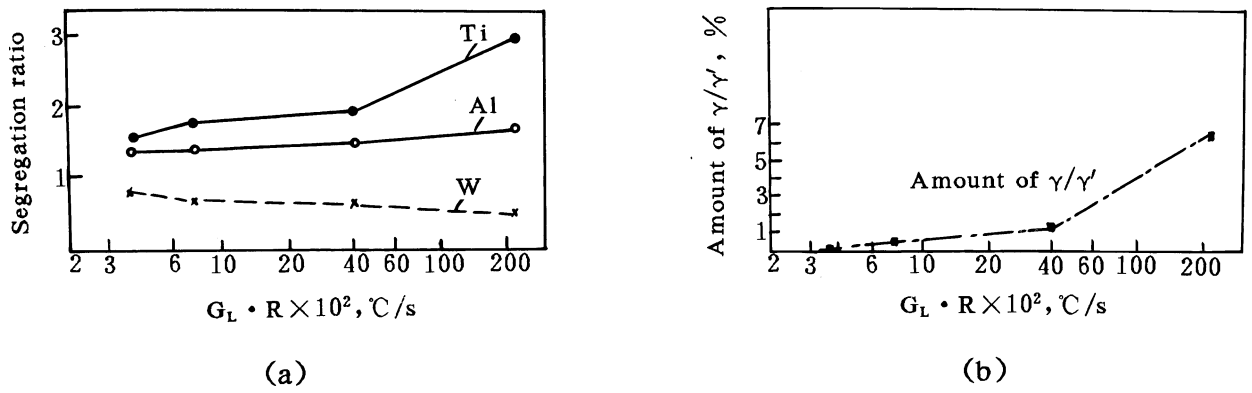

Fig. 4—Influences of the solidification cooling rate ($G_L \cdot R$) on (*a*) Al, Ti, and W segregation ratios and (*b*) the amount of γ/γ' eutectic in as-cast microstructure.

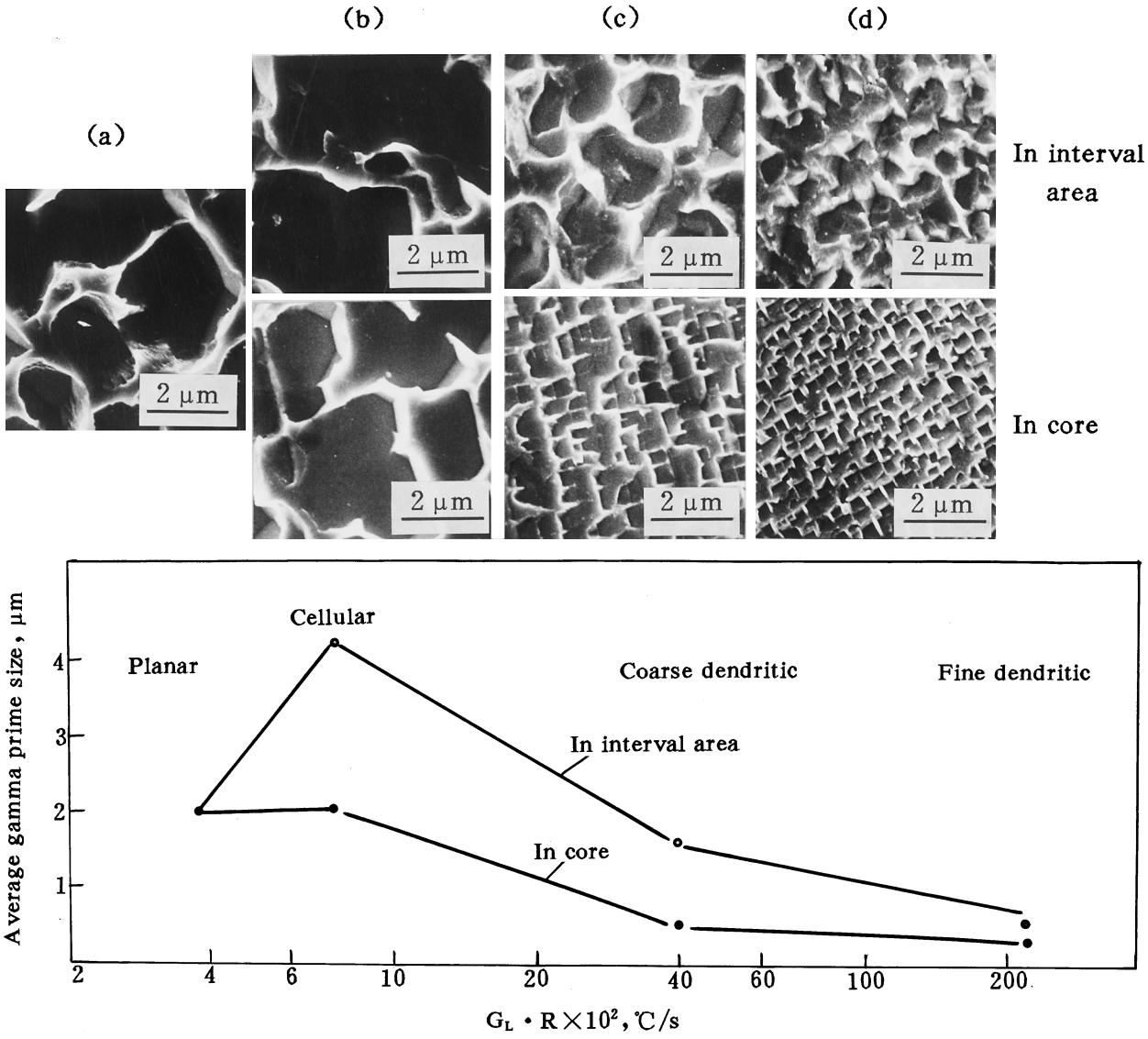

Fig. 5—Effect of solidification cooling rates on the morphology and average size of as-cast γ' precipitates. SEM micrographs of (*a*) planar, (*b*) cellular, (*c*) coarse-dendritic, and (*d*) fine-dendritic single crystals of NASAIR 100.

heat treatment at 1320 °C for 4 hours, and AC, the average stress-rupture life of both the coarse-dendritic and the fine-dendritic single crystals was further improved. For all material conditions, the longest average stress-rupture life, 228 hours, belonged to the coarse-dendritic single crystals heat treated at 1320 °C for 4 hours, and AC. Explicitly, the planar and the cellular single crystals did not exhibit superiority over the dendritic single crystals in stress-rupture life.

Table III. Average Size and Morphology of γ' and the Amount of γ/γ' Eutectic in As-Cast NASAIR 100

Solidification Cooling Rate $G_L \cdot R$ (°C/s)	Average Size (μm) and the Morphology of γ'		Amount of γ/γ' Eutectic (Area Pct)
	In Cores	In Intervals	
3.75×10^{-2} planar	2.2 irregular		0
7.25×10^{-2} cellular	2.0 irregular	4.2 very irregular	0.6
3.88×10^{-1} coarse-dendritic	0.45 cubic	1.40 cubic trend	1.3
2.18 fine-dendritic	0.25 cubic	0.45 cubic	6.5

E. *Discussion*

1. *As-cast microstructure*

In the present work, the single crystals of NASAIR 100 contained more than 93 pct γ solid solution with either only a small amount, or none, of the γ/γ' eutectic just at the end of solidification. However, at temperatures below the γ' solvus, the γ solid solution became supersaturated, and then a diffusion-controlled precipitating phase transformation started, as follows:

$$\gamma_1 \rightarrow \gamma_2 + \gamma' \qquad [3]$$

where γ_1 is the original supersaturated γ solid solution, and γ_2 is the retained γ solid solution after γ' has precipitated. The critical radius, r^*, and the apparent activation energy, ΔG^*, for the homogeneous nucleation of a γ' precipitate could be expressed as follows:[13]

$$r^* = \frac{2\rho_{\gamma-\gamma'}}{\Delta G_v - \Delta G_\varepsilon} \qquad [4]$$

$$\Delta G^* = \frac{16\pi\rho^3_{\gamma-\gamma'}}{3(\Delta G_v - \Delta G_\varepsilon)^2} \qquad [5]$$

where $\rho_{\gamma-\gamma'}$ represents the surface-tension energy per unit area of $\gamma - \gamma'$ interface; ΔG_v and ΔG_ε are, respectively, the differential free energy and the differential strain energy for precipitating per unit volume of γ' phase. Additionally, ΔG_v is proportional, respectively, to the supercooling degree, ΔT, and to the supersaturation degree, ΔC, of γ solid solution.[14]

It is well known that the diffusion-controlled phase transformation needs a certain incubation period.[15] In the supersaturated γ solid solution of NASAIR 100, just below the γ' solvus, poor solute zones and abundant solute zones formed first at the incubation period, creating favorable compositional conditions to precipitate γ' particles. It was because of the prerequisite of a certain incubation period that a rapid cooling needed a large temperature fall, and thus lowered the beginning temperature to form γ' precipitates, resulting in an increase in ΔT.[13,14,15] According to Eq. [5] and Xiao's work,[14] this decreased ΔG^*, and improved the nucleation rate of γ' precipitates per unit volume of supersaturated γ solid solution.

With the transition of samples' S/L interfaces from the planar to the cellular, coarse-dendritic, and finally to the fine-dendritic morphology, the nucleation rate of γ' precipitates increased, because of the improved cooling rate of supersaturated γ solid solution by the rising $G_L \cdot R$. Furthermore, the time to allow the growth of γ' precipitates at high temperatures decreased with the aforementioned successive morphology transition of S/L interfaces. Therefore, the size of γ' precipitates reduced gradually.

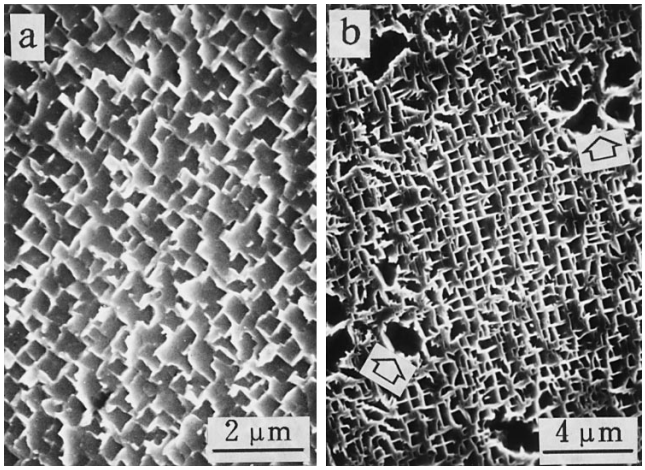

Fig. 6—Heat-treated microstructure of the planar single-crystal NASAIR 100 (*a*) after heat treatment at 1280 °C/4 h, AC and (*b*) heat treated at 1320 °C/4 h, AC. Note the presence of large irregular blocks (arrow).

It is also illustrated in Figure 5 that the γ' precipitates were larger in interval areas than in crystallizing cores. The γ' forming elements, such as Al, Ti, and Ta, were positively segregated and enriched in interval areas, which caused a larger supersaturation, ΔC, and thus reduced ΔG^* in interval areas. Therefore, γ' particles could start to precipitate at higher temperatures, and there was a longer time for the growth of γ' at high temperatures in interval areas than in crystallizing cores of the same sample. Furthermore, the driving force for the growth of γ' was larger in interval areas than in crystallizing cores, also due to the larger ΔC. It was for these two reasons that the γ' precipitates in interval areas were larger.

The theories of solid-phase transformation show that the morphologies of precipitates are controlled by the surface-tension energy and the strain energy of the precipitates.[14,16,17] Following this opinion, one possible explanation for the observed γ' morphologies is that when γ' is small, the $\gamma - \gamma'$ interface area per unit volume γ' is large, and thus the surface-tension energy is the predominant action factor on the γ' shape. In this case, cubic γ' with a coherent $\gamma - \gamma'$ interface is present because of its very low surface-tension energy. Instead, when γ' is large, the $\gamma - \gamma'$ interface area per unit volume γ' is small, and thus the strain energy is predominant. This makes irregular γ', with a less coherent $\gamma - \gamma'$ interface present, so as to reduce the strain energy. Therefore, the γ' precipitates in both the planar and the cellular single crystals of NASAIR 100 were irregular, just like an ''overaged'' microstructure, because of their large sizes resulting from lower cooling rates; however, in the dendritic single crystals, the γ' precipitates tended to be cuboidal, especially in the dendrite cores. Further detailed work is required, however, to verify this inference.

Figures 4(a) and (b) show that microsegregation and the amount of γ/γ' eutectic in the as-cast microstructure in-

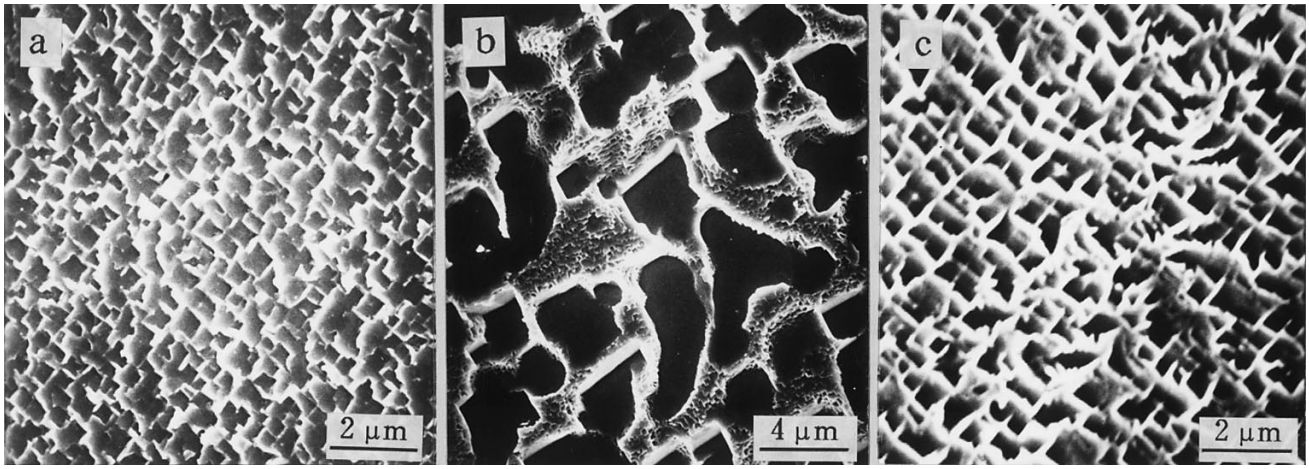

Fig. 7—SEM micrographs of the heat-treated cellular single-crystal NASAIR 100 (*a*) heat treated at 1280 °C/4 h, AC, in the cellular core; (*b*) heat treated at 1280 °C/4 h, AC, in the cellular interval; and (*c*) 1320 °C/4 h, AC heat treated.

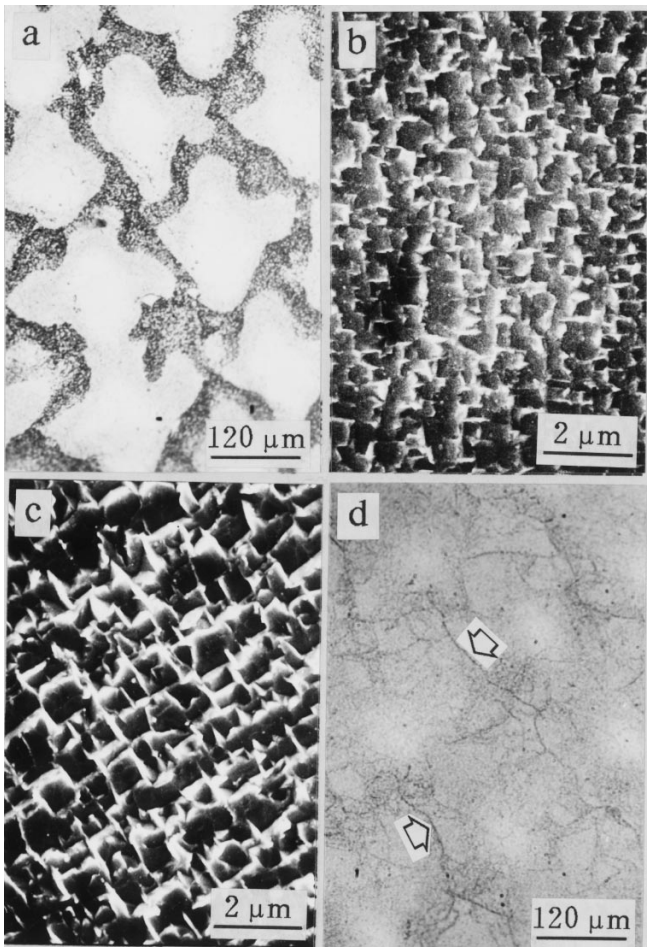

Fig. 8—Heat-treated microstructure of a coarse-dendritic NASAIR 100 single crystal. (*a*) Optical micrograph showing that dendritic patterns were still clear after 1280 °C/4 h, AC. (*b*) SEM micrograph showing uniform cubic γ' after 1300 °C/4 h, AC treatment. (*c*) Reprecipitated γ' (SEM) and (*d*) optical micrograph after 1320 °C/4 h, AC treatment. Note the absence of dendritic patterns and the presence of subgrain boundaries (arrow).

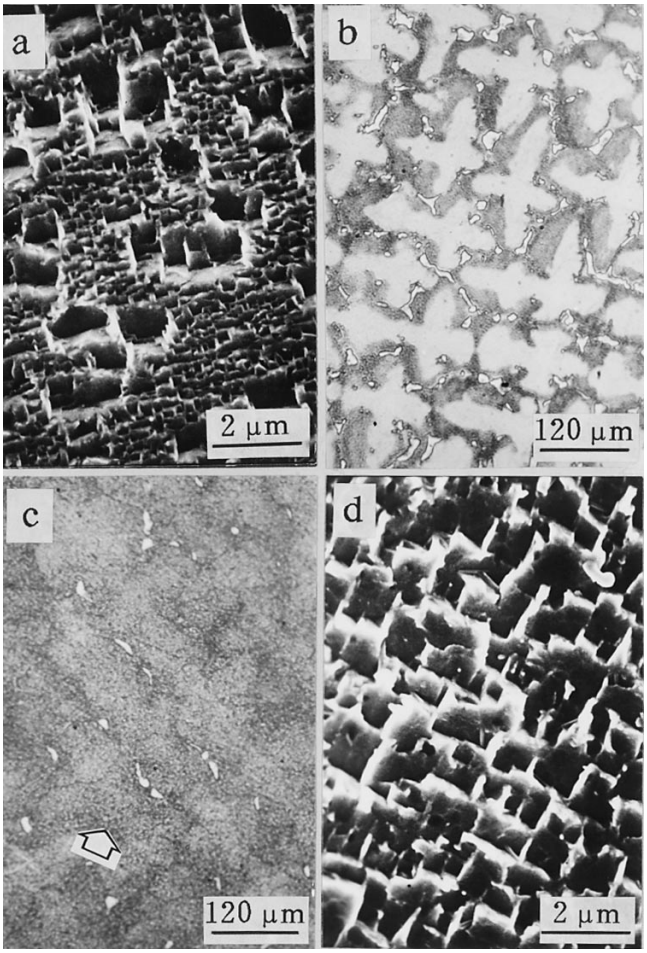

Fig. 9—Heat-treated microstructure of the fine-dendritic NASAIR 100 (*a*) heat treated at 1280 °C/4 h, AC, in interdendritic area. (*b*) Optical micrograph after 1300 °C/4 h, AC treatment. (*c*) Optical micrograph showing remaining dendritic patterns after 1320 °C/4 h, AC treatment. (*d*) Reprecipitated γ' cubes after 1320 °C/4 h, AC treatment.

crease with the successive transition of S/L interfaces from the planar to the cellular, coarse-dendritic, and finally to the fine-dendritic morphology. This is seemingly opposite to the results of Fritzemeier, where microsegregation and the amount of γ/γ' eutectic decrease when going from coarse- to fine-dendritic structure.[7] The reason for this superficial contradiction is the different processing manners when go-

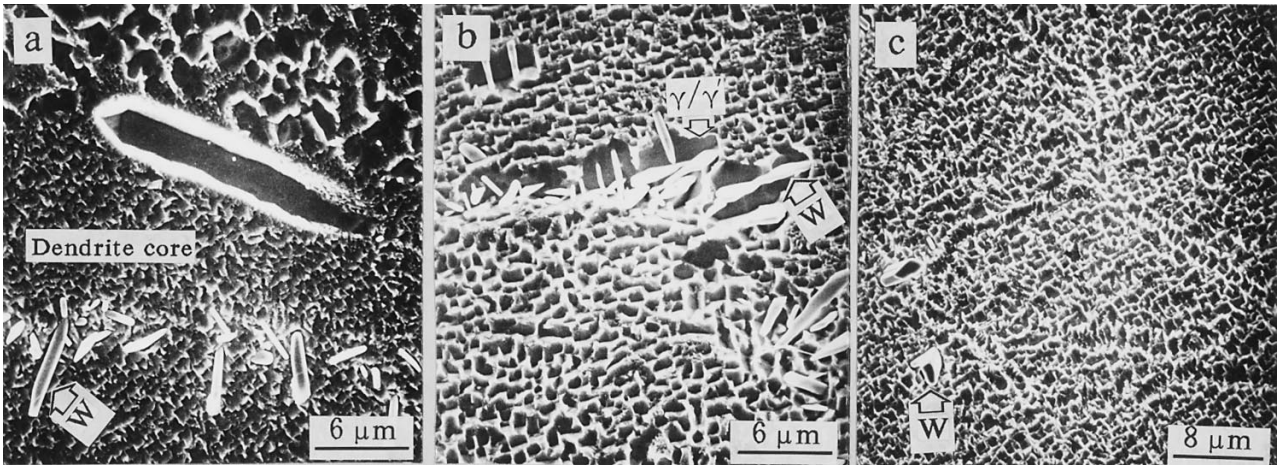

Fig. 10—Scanning electron micrographs showing the presence of W-rich plates in dendritic NASAIR 100 after solution heat treatments. (*a*) Coarse-dendritic NASAIR 100 heat treated by 1280 °C/4 h, AC. (*b*) Fine-dendritic NASAIR 100 heat treated by 1280 °C/4 h, AC. (*c*) Coarse-dendritic NASAIR 100 heat treated by 1320 °C/4 h, AC.

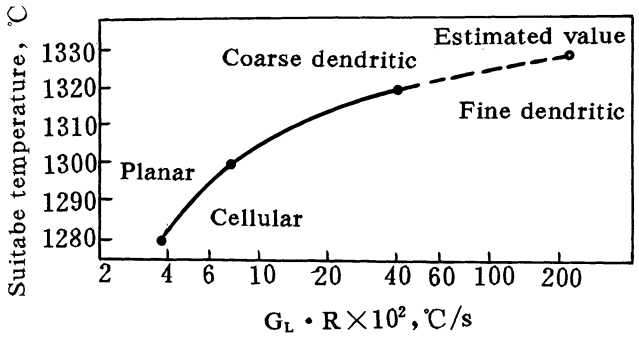

Fig. 11—Effect of solidification cooling rates on the solution temperature required to dissolve all as-cast γ' and most of the γ/γ' eutectic and to homogenize compositional microsegregation (holding for 4 h at each temperature).

ing from the coarse- to the fine-dendritic structure. Although in both cases the solidification cooling rates increased, in Reference 7, higher thermal gradient casting resulted in the fine-dendritic structure; in contrast, increased withdrawal rate at a constant thermal gradient of 250 ± 5 °C/cm produced the fine-dendritic S/L interface in the present work.

It is well known that in the common range of solidification cooling rates, in which solute trapping does not occur and the solute redistribution factor can be considered approximately constant, the chemical microsegregation is mainly determined by the homogenizing effects of diffusion in the solidifying solid solution, which depends upon two influencing factors: diffusion time at high temperatures and diffusion distances.[13,18] An increased solidification cooling rate has two contradictory effects on microsegregation. On the one hand, it decreases the diffusion time at high temperatures of the solid solution in the mushy zone, resulting in an increase in microsegregation. On the other hand, it reduces the DAS and decreases the diffusion distances, resulting in a reduction in microsegregation.

In Reference 7, since it was induced by increased thermal gradient casting, which mainly reduced DAS, the transition from the coarse- to the fine-dendritic structure decreased both microsegregation and the amount of γ/γ' eutectic. Instead, since it was accomplished by increased withdrawal rate at a constant thermal gradient, both the DAS and the diffusion time were reduced in the present work. However, the reduction in diffusion time was predominant in determining the diffusional effects in this situation, since the solidification cooling rate, $G_L \cdot R$, was not large enough, and thus DAS was not reduced so significantly as to counteract the reduction in diffusion time. Therefore, the microsegregation and the amount of γ/γ' eutectic increased with the transition from the coarse- to the fine-dendritic structure in the present work.

2. *Solution behavior and heat-treated microstructure*

It is shown in Figure 11 that with the successive transition of S/L interfaces from the planar to the cellular, coarse-dendritic, and finally to the fine-dendritic morphologies, the solution temperature required to dissolve all coarse as-cast γ' precipitates and most of the γ/γ' eutectic increased, when the holding time at each solution temperature was constantly 4 hours. The reason was that the microsegregation and amount of γ/γ' eutectic produced in solidification processes increased with the aforementioned successive transition of S/L interfaces. Therefore, more effective diffusion at higher solution temperatures was needed so as to homogenize the increased microsegregation and to dissolve the increased γ/γ' eutectic.

In the present work, the reprecipitated γ' after solution heat treatments was obviously smaller than the as-cast γ' in both the planar and the cellular single crystals of NASAIR 100. However, in the fine-dendritic single crystals of NASAIR 100, the reprecipitated γ' in dendrite cores after 1280 °C and 1300 °C heat treatments, and in overall area after 1320 °C heat treatment, was larger than the as-cast γ' in the corresponding areas. The sizes of γ' precipitates were controlled by the cooling rate of samples from the γ' solvus to about 1090 °C. High cooling rates produced fine γ' precipitates.[19] As the solidification cooling rate of the fine-dendritic single crystals was relatively high ($G_L \cdot R = 2.18$ °C/s), even higher than the common AC rate from 1280 °C (estimated as 1.67 °C/s), the reprecipitated γ' after 1280 °C solution heat treatment was larger than the as-cast γ'. Moreover, since it made the samples preheat the surrounding air environment more effectively, and thus the heat-diffusion rate from them was reduced, the higher solution tempera-

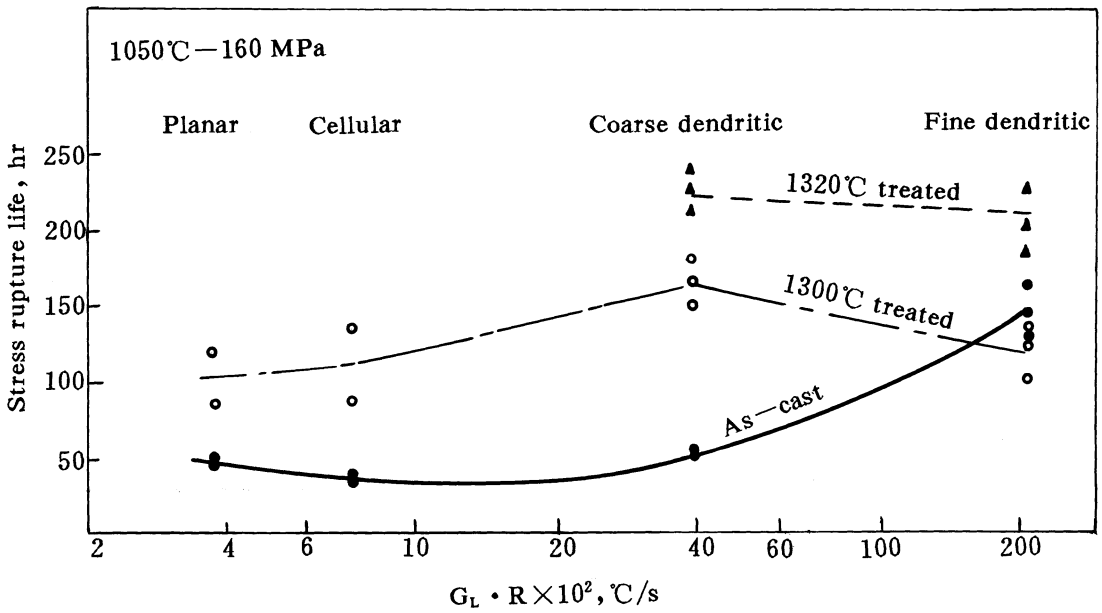

Fig. 12—High-temperature stress-rupture life of single-crystal NASAIR 100 at 1050 °C and 160 MPa *vs* solidification cooling rates.

Table IV. Stress-Rupture Lives at 1050 °C and 160 MPa and Their Corresponding Initial Microstructure of NASAIR 100*

$G_L \cdot R$ (°C/s)		Solution Heat Treatments		
		As-Cast	1300 °C/4h, AC	1320 °C/4h, AC
3.75×10^{-2} planar	structure:	γ': 2.2 μm and irregular	0.36 μm and cubic	0.42 μm and cubic some big blocks of γ' (1.7 μm)
	life (h):	50.3, 43.1	87.2, 121.3	—
7.25×10^{-2} cellular	structure:	γ': 2.0 μm in cores; 4.2 μm in intervals; and very irregular; 0.6 pct γ/γ'	0.33 μm and cubic	0.53 μm and cubic
	life (h):	33.8, 40.7	88.7, 138.5	—
3.88×10^{-1} coarse-dendritic	structure:	γ': 0.45 μm, cubic in cores; and 1.40 μm, cubic trend in intervals 1.3 pct γ/γ'	0.38 μm and cubic 0.3 pct γ/γ' 0.7 pct W-rich phase	0.57 μm and cubic 0.1 pct γ/γ' 0.1 pct W-rich phase
	life (h):	51.3, 55.5	151.7, 165.5, 182.3,	214.8, 227.8, 242.3
2.18 fine-dendritic	structure:	γ': 0.25 μm in cores; and 0.45 μm in intervals, cubic 6.5 pct γ/γ'	0.35 μm in cores; and partial solution in intervals, cubic residual segregation 5.7 pct γ/γ' 3.5 pct W-rich phase	0.56 μm and cubic residual segregation 2.2 pct γ/γ' 0.3 pct W-rich phase
	life (h):	129.7, 145.0, 162.3	102.0, 124.5, 125.3	196.5, 199.0, 231.5

*Stress rupture tests were not conducted for the single crystals heat treated at 1280 °C/4 h, AC, but the microstructural features after these heat treatments have been described in the text.

ture lowered the cooling rate from the γ' solvus to about 1090 °C, resulting in larger reprecipitated γ'.

The formation of the W-rich phase was partly attributable to the microsegregation produced in the nonequilibrium solidification process.[20] After SHT, the W-rich phase was observed in neither the planar nor the cellular single crystals of NASAIR 100 with relatively slight microsegregation. However, in the dendritic single crystals of NASAIR 100, the W-rich phase was present after SHT, because of serious microsegregation.

The reduction of the W-rich phase after solution heat treatment at a higher temperature was a result of the more sufficient homogenization of segregation by faster diffusion. However, the W-rich phase was not observed in the as-cast microstructure, although as-cast segregation was most serious, because the formation of the W-rich phase required not only certain segregation, but also certain time and temperature conditions for nucleation and growth.

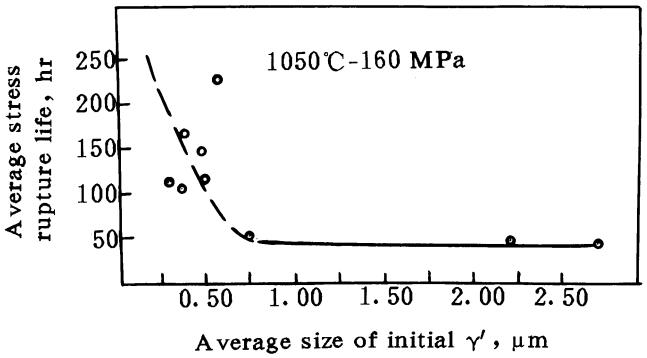

Fig. 13—Relationship between the average stress rupture life and the average size of initial γ' precipitates under various conditions of the single crystals of NASAIR 100.

3. *Microstructural characteristics to affect stress-rupture life*

As is well known, the size and shape of γ' precipitates exert significant influence on the elevated-temperature stress-rupture properties of single-crystal superalloys.[20,21] Figure 13 presents the relationship between the average stress-rupture life and the average size of corresponding initial γ' precipitates (γ' before stress-rupture tests) of various single crystals of NASAIR 100, where the average size of initial γ' was determined from quantitative metallography measurements. The other microstructural features are also summarized in Table IV, together with the corresponding stress-rupture lives. Although the stress-rupture life is also affected by other microstructural characteristics, such as the amount of γ/γ' eutectic and of the W-rich phase, and the stability of γ' precipitates, which are difficult to consider in the same figure, Figure 13 still illustrates that the average size of initial γ' significantly influenced the average stress-rupture life of the single crystals of NASAIR 100, and when it was larger than about 0.60 μm, the average stress-rupture life was lowered dramatically. Moreover, the initial γ' precipitates with cubic edges were usually developed into perfect γ' rafts during high-temperature creep, which improved creep resistance.[21,22,23] Therefore, fine and cuboidal γ' precipitates exhibited effective strengthening.

The second influencing factor on stress-rupture life may be the amount and size of both the γ/γ' eutectic and the W-rich phase. Duhl has pointed out that topologically closed packed (TCP) phases such as σ, μ, or Laves are less detrimental in single-crystal superalloys than in polycrystalline alloys, because the alloy matrix of the former material is inherently more ductile.[19,24] However, other investigators have found that the precipitation of the W-rich μ phase lowers the creep resistance of the MXON alloy.[25] In the present work, although compared to the as-cast condition, the microsegregation was weakened, and the sizes and shapes of γ' were not changed substantially, the stress-rupture life of the fine-dendritic single crystals of NASAIR 100 reduced explicitly after the solution treatment at 1300 °C. Hence, the precipitation of 3.5 pct (area pct) W-rich plates with sharp edges is thought to be partly responsible for decreasing the stress-rupture life. The detrimental effect of this phase could result from (1) the partial depletion of the matrix in W and Mo which, are originally important strengthening elements;[19,24] and (2) its embrittlement, resulting in the easier initiation of cracks.[26]

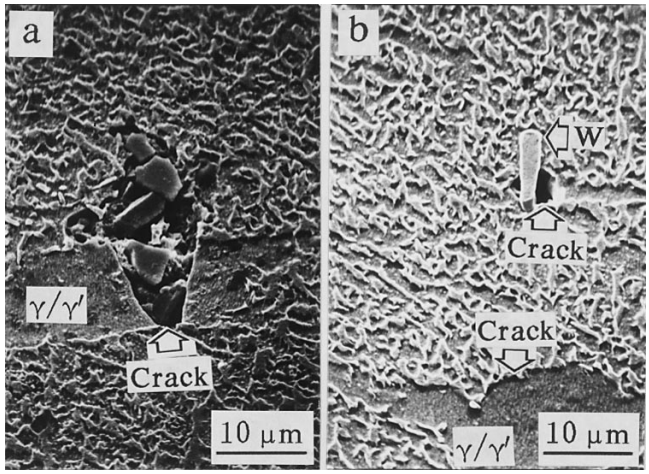

Fig. 14—Scanning electron micrographs showing cracks preferentially initiated at (*a*) γ/γ' eutectic and (*b*) W-rich plates.

Moreover, γ/γ' eutectic is also detrimental to the stress-rupture life because of its larger size and vulnerability at high temperatures.[7,24,26] These are further verified by Figure 14, which shows that some relatively large cracks initiated preferentially at γ/γ' eutectic islands and W-rich plates. Although creep voids in single-crystal superalloys are generally not observed until third-stage creep,[7,20,24,26] an increased amount and size of γ/γ' eutectic and W-rich plates may advance the onset of the tertiary creep, undoubtedly producing a reduction in the stress-rupture life of the single crystals.

The third factor to influence the stress-rupture life of the single crystals of NASAIR 100 was the coarsening behavior of initial γ' precipitates during high-temperature stress-rupture tests. Some studies[20–23, 27–29] have revealed that perfect γ' rafts effectively suppressed not only the climbing but also the looping mechanisms of dislocations, because of the dramatic reduction of vertical γ-γ' interfaces (parallel to the tensile axis), and made the more difficult γ' shearing mechanism operative, resulting in improved creep resistance. In the present work, although the initial γ' precipitates (γ' prior to stress-rupture tests) in both the planar and the cellular single crystals were similar to those in the coarse-dendritic single crystals in the aspects of their size and shape after heat treatment at 1300 °C for 4 hours, and AC, both average stress-rupture lives of the former two kinds of single crystals were explicitly shorter than that of the latter. This was because the γ' rafts formed during stress-rupture tests at 1050 °C in the former two kinds of materials were much thicker, not perfect, and with lower average aspect ratios (Figures 15(a) and (b)), resulting in a reduction in the creep resistance. Instead, the γ' rafts in the 1300 °C heat-treated coarse-dendritic single crystals were more perfect and with a high average aspect ratio; additionally, their width was only slightly larger than the edge length of the initial γ' cubes, resulting in improved stress-rupture resistance[13] (Figure 15(c)). The aforementioned difference in the width and morphology of γ' rafts perhaps resulted from the partial hereditary tendency of the original coarse as-cast γ' precipitates in the planar and cellular single crystals. Although fine dispersed cuboidal γ' precipitates were produced after SHT, it was easier for them to coarsen to the original as-cast morphology and size under suitable con-

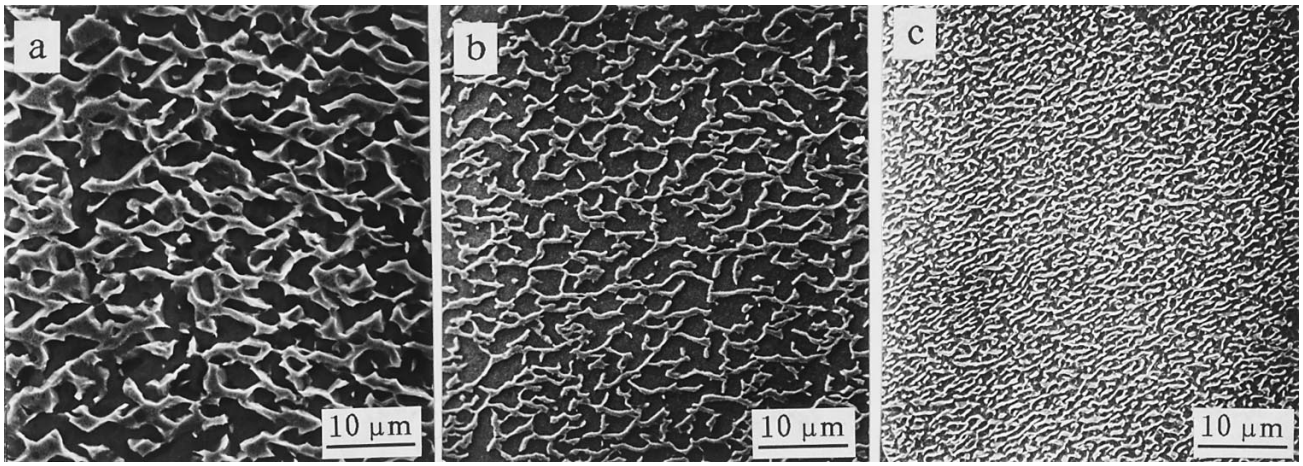

Fig. 15—Longitudinal microstructure of 1300 °C/4 h, AC treated samples stress-ruptured at 1050 °C and 160 MPa. Samples with (*a*) the planar, (*b*) the cellular, and (*c*) the coarse-dendritic S/L interface morphologies. All micrographs were taken at sites 3.5 mm away from the fractured surfaces. The dark platelets are γ' rafts. The stress axis is vertical.

ditions, such as exposure to elevated temperatures for a long time in both the planar and cellular single crystals of NASAIR 100. This was further verified by the large γ' blocks that appeared in the 1320 °C heat-treated microstructure of the planar single crystals (Figure 6(b)). On the other hand, some oriented coarsening of initial γ' should proceed in a uniaxial stress at high temperatures.[20–23,27] As a result of the interaction of hereditary coarsening and oriented coarsening, thicker and less perfect γ' rafts formed in both the planar and cellular single crystals. However, further research is required to completely understand this difference in γ' raft morphology.

Now we can explain the variation of the stress-rupture lives at 1050 °C and 160 MPa of the single crystals of NASAIR 100 with the transition of S/L interface morphologies shown in Figure 12. In the as-cast condition, although the amount of γ/γ' eutectic increased with the transition of S/L interface from the planar to the coarse-dendritic, and finally to the fine-dendritic morphology, the average stress-rupture life of the single crystals of NASAIR 100 improved progressively. The reason was that the average size of γ' precipitates decreased, and their shapes tended to become cuboidal with the aforementioned transition of S/L interface. Additionally, the average stress-rupture life of the as-cast cellular single crystals was the shortest because of the largest initial γ' precipitates with very irregular shape. After heat treatment at 1300 °C for 4 hours, and AC, the reprecipitated γ' was fine and cuboidal; furthermore, γ/γ' eutectic was hardly observed in all the planar, cellular, and coarse-dendritic single crystals of NASAIR 100. So, the three average stress-rupture lives were significantly improved by this heat treatment. Besides, the average stress-rupture life of the coarse-dendritic single crystals was the highest because of the extra microstructural advantage of the more perfect and thinner γ' rafts formed during stress-rupture tests (Figure 15(c)). However, the average stress-rupture life of the fine-dendritic single crystals decreased after the 1300 °C heat treatment. The reason was that the amount of residual γ/γ' eutectic was still as much as 5.7 pct, microsegregation was still present, and, more seriously, a relatively large amount (3.5 pct, in area percent) of sharp W-rich phase was formed. By heat treatment at 1320 °C for 4 hours, and AC, both average stress-rupture lives of the coarse- and fine-dendritic single crystals were further improved, based on the following three reasons: (1) only a small amount of W-rich plates was present in the microstructure; (2) γ/γ' eutectic was almost eliminated in the coarse-dendritic single crystals, and was dramatically reduced in the fine-dendritic single crystals; and (3) the initial γ' was cuboidal, its average size was smaller than 0.60 μm, and, more importantly, perfect γ' rafts formed during creep.

4. *Influence of solidification cooling rate on stress-rupture life*

The experimental results in the present work evidenced that the solidification cooling rate indeed exerted an explicit influence on the high-temperature stress-rupture life (Figure 12). This influence still existed even if the alloys were then solution heat treated, and the initial microstructure in the alloys consisted of the γ' precipitates with nearly the same size and shape, as listed in Table IV.

The physical properties are generally controlled by the corresponding microstructure, which mainly consists of γ' precipitates in γ matrix, and sometimes with a limited amount of γ/γ' eutectic and TCP phases in single-crystal superalloys.[1,2,13] Hence, the size and morphology of γ' precipitates and their coarsening behavior during stress-rupture tests are very important factors to finally determine the stress-rupture life.[13,20,27] However, not only postsolidification SHT cooling rates, but also the solidification cooling rates affect the finally microstructural features. In the present work, solidification cooling rates had three effects: (1) to determine as-cast microstructure (Figures 4 and 5); (2) to influence SHT behavior (Figure 11); and (3) to affect the coarsening behavior of initial γ' precipitates during stress-rupture tests (Figure 15). The last effect of solidification cooling rates resulted in the dendritic single crystals originally containing the highest microsegregation having the longest stress-rupture life after suitable SHT, which could effectively homogenize the microsegregation. The main reason was that the γ' rafts formed during the stress-rupture tests of the dendritic single crystals were much

more perfect and thinner than those in both the planar and cellular single crystals, although the initial γ' precipitates were nearly the same in the aspects of size and shape in all single crystals. However, the reasons for these observed differences in the coarsening behavior during stress-rupture tests are not clear at this time, but the very coarse as-cast γ' precipitates, due to very slow solidification cooling rates in both the planar and cellular single crystals, may be contributing factors. Thus, it is possible that solidification cooling rates may have some permanent effects on the final microstructure and stress-rupture life. This is further verified by current research, which has shown that ultrahigh solidification cooling rates can significantly improve the elevated-temperature stress-rupture strength of the superalloy DZ 22, even if postsolidification SHT was employed.[30]

IV. CONCLUSIONS

1. At a constant temperature gradient of 250 ± 5 °C/cm, the single crystals of NASAIR 100, with various S/L interfaces (planar, cellular, coarse-dendritic, and fine-dendritic), were obtained by varying the withdrawal rate within a wide range.
2. With the successive transition of the S/L interface from the planar to the cellular, coarse-dendritic, and finally to the fine-dendritic morphology, microsegregation extent and γ/γ' eutectic produced in the solidification process increased, the average γ' size decreased, and the γ' shape successively turned cubic, in the as-cast microstructure. Moreover, the as-cast γ' precipitates were larger in interval areas than in crystallizing cores.
3. The reasons for finer γ' precipitates in as-cast dendritic single crystals were that the nucleation rate of γ' precipitates increased and the time to allow the growth of γ' precipitates decreased, because of the improved cooling rate of supersaturated γ solid solution by the rising $G_L \cdot R$. Larger γ' precipitates in interval areas of as-cast structure resulted from larger supersaturation of ΔC. Furthermore, fine γ' precipitates usually had a cubic shape.
4. The solution temperature required to dissolve all as-cast γ' precipitates and most of the γ/γ' eutectic increased with increasing $G_L \cdot R$, when holding time at each temperature was constantly 4 hours. Reprecipitated γ' upon AC was usually fine, dispersed, and cuboidal. The W-rich phase was only present in the dendritic single crystals of NASAIR 100 after SHT.
5. In the as-cast condition, the fine-dendritic single crystals exhibited the longest average stress-rupture life. After heat treatment at 1300 °C for 4 hours, and AC, all average stress-rupture lives of the planar, cellular, and coarse-dendritic single crystals increased significantly, with that of the coarse dendritic being the highest. However, this heat treatment lowered the average stress-rupture life of the fine-dendritic single crystals. The heat treatment of 1320 °C for 4 hours, and AC, further improved the average stress-rupture life of both the coarse-dendritic and the fine-dendritic single crystals.
6. Fine, cuboidal, and stable γ' precipitates exerted effective strengthening. The γ/γ' eutectic and W-rich plates provided preferential sites to initiate cracks, and were detrimental to the high-temperature stress-rupture strength.

ACKNOWLEDGMENTS

The authors express their deep gratitude to the NSFC (Natural Science Foundation of China) for support of this work. A sincere appreciation is extended to Professor Zhengxing Shi, Northwestern Polytechnical University, and to Mr. Chaoying Hui, Northwestern University (Xi' an) for providing support and helpful discussions. Thanks are also due to Professor Dr. Lin Liu, Northwestern Polytechnical University, for valuable comments.

REFERENCES

1. M. Gell, D.N. Duhl, and A.F. Giamei: in *Superalloys 1980*, Proc. 4th Int. Symp. on Superalloys, J.K. Tien, S.T. Wlodek, H. Morrow III, M. Gell, and G.E. Maurer, eds., ASM, Metals Park, OH, 1980, pp. 205-14.
2. G.S. Hoppin II and W.P. Danesi: in *Superalloys II, High Temperature Materials for Aerospace and Industrial Power*, C.T. Sims, N.S. Stoloff, and W.C. Hagel, eds., a Wiley-Interscience Publication, John Wiley & Sons, New York, NY, 1987, pp. 949-62.
3. A.D. Cetel and D.N. Duhl: in *Superalloys 1988*, Proc. 6th Int. Symp. on Superalloys, S. Reichman, D.N. Duhl, G. Maurer, S. Antolovich, and C. Lund, eds., TMS, Warrendale, PA, 1988, pp. 235-44.
4. D. Blavette, P. Caron, and T. Khan: in *Superalloys 1988*, Proc. 6th Int. Symp. on Superalloys, S. Reichman, D.N. Duhl, G. Maurer, S. Antolovich, and C. Lund, eds., TMS, Warrendale, PA, 1988, pp. 305-14.
5. Zhang Zhuqian, Liu Zhizhong, and Sun Ying: *J. Univ. Sci. Technol. Beijing*, 1991, vol. 13 (10), pp. 42-52 (in Chinese).
6. G.L. Leatherman and R. Nathan Katz: in *Superalloys, Supercomposites and Superceramics*, J.K. Tien and T. Caulfield, eds., Academic Press, Inc., New York, NY, and Harcourt Brace Jovanovich, Sidcup, Kent, United Kingdom, 1989, pp. 671-96.
7. L.G. Fritzemeier: in *Superalloys 1988*, Proc. 6th Int. Symp. on Superalloys, S. Reichman, D.N. Duhl, G. Maurer, S. Antolovich, and C. Lund, eds., TMS, Warrendale, PA, 1988, pp. 265-74.
8. Tang Dingzhong, Zhong Zhengang, Dai Xiuyan, and Wu Zhongtang: in *Proc. China Nat. Conf. on Superalloys*, Zhong Zhenyong, Yang Jinyan, Sun Jiahua, Ma Peili, Li Hankang, and Yuan Ying, eds., The Metal Society of China, Beijing, 1987, pp. 805-08 (in Chinese).
9. J. Gayda and R.A. MacKay: *Scripta Metall.*, 1989, vol. 23, pp. 1835-38.
10. T. Khan: in *High Temperature Alloys for Gas Turbines and Other Applications*, W. Betz, R. Brunetaud, D. Coutsouradis, H. Fischmeister, T.B. Gibbons, and I. Kvernes, eds., D. Reidel Publishing Co., Dordrecht, The Netherlands, 1986, pp. 729-43.
11. J.K. Tien and R.P. Gamble: *Mater. Sci. Eng.*, 1971, vol. 8, pp. 152-60.
12. M. Gell and D.N. Duhl: in *Processing and Properties of Advanced High Temperature Alloys*, S.M. Allen, R.M. Pelloux, and R. Widmer, eds., ASM, Metals Park, OH, pp. 41-49.
13. Guo Xiping: Ph.D. Thesis, Northwestern Polytechnical University, Xi'an, People's Republic of China, 1992, Jan., pp. 29-56 (in Chinese).
14. Xiao Jimei: *Alloy Phase and Its Transformation*, The Chinese Metallurgical Publishing House, Beijing, 1987, pp. 233-35 (in Chinese).
15. T. Khan: in *High Temperature Alloys for Gas Turbines and Other Applications*, W. Betz, R. Brunetaud, D. Coutsouradis, H. Fischmeister, T.B. Gibbons, and I. Kvernes, eds., D. Reidel Publishing Co., Dordrecht, The Netherlands, 1986, pp. 21-50.
16. Peter Haasen: *Physical Metallurgy*, Cambridge University Press, Cambridge, United Kingdom, 1978, pp. 194-219.
17. R.A. MacKay and M.V. Nathal: NASA TM-88788, National Technical Information Services, Springfield, VA, 1986, pp. 1-37.
18. J.J. Montoya-Cruz, R. Kadalbal, T.Z. Kattamis, and A.F. Giamei: *Metall. Trans. A*, 1982, vol. 13A, pp. 1153-59.
19. D.N. Duhl: in *Superalloys, Supercomposites and Superceramics*, J.K. Tien and T. Caulfield, eds., Academic Press, Inc., New York, NY, and Harcourt Brace Jovanovich Publishers, Sidcup, Kent, United Kingdom, 1989, pp. 149-82.
20. M.V. Nathal and L.J. Ebert: *Metall. Trans. A*, 1985, vol. 16A, pp. 427-39.

21. R.A. MacKay and L.J. Ebert: NASA TM-83595, National Technical Information Services, Springfield, VA, 1984, pp. 1-10.
22. P. Caron, P.J. Henderson, T. Khan, and M. Mclean: *Scripta Metall.*, 1986, vol. 20, pp. 875-80.
23. P. Caron and T. Khan: *Mater. Sci. Eng.*, 1983, vol. 61, pp. 173-84.
24. D.N. Duhl: in *Alloy Phase Stability and Design*, G.M. Stocks, D.P. Pope, and A.F. Giamei, eds., Materials Research Society, Pittsburgh, PA, 1991, pp. 389-99.
25. T. Khan, P. Caron, and C. Duret: in *Superalloys 1984*, Proc. 5th Int. Symp. on Superalloys, M. Gell, C.S. Kortovich, R.H. Bricknell, W.B. Kent, and J.F. Radavich, eds., AIME, New York, NY, 1984, pp. 145-54.
26. Guo Xiping and Fu Hengzhi: *Z. Metallkd.*, 1996, Band 87, pp. 315-20.
27. R.A. MacKay and L.J. Ebert: *Metall. Trans. A*, 1985, vol. 16A, pp. 1969-82.
28. M.V. Nathal and L.J. Ebert: *Metall. Trans. A*, 1985, vol. 16A, pp. 1849-62.
29. M.V. Nathal and L.J. Ebert: *Metall. Trans. A*, 1985, vol. 16A, pp. 1863-70.
30. Liu Zhongyuan, Li Jianguo, Shi Zhengxing, Fu Hengzhi, She Li, Chen Rongzhang, and Wang Luobao: *J. Mater. Eng.*, 1995, No. 145, pp. 15-18 (in Chinese).